THE VORTEX STRUCTURE FORMATION AROUND A CIRCULAR CYLINDER PLACED ON A VERTICAL HEATED PLATE

Yu.S. Chumakov, A.M. Levchenya, H. Malah

Peter the Great St. Petersburg Polytechnic University, St. Petersburg, Russian Federation

The interaction process analysis and results of numerical simulation of a free-convection boundary layer developing around a circular cylinder placed on a vertical heated plate are presented. The cylinder axis is directed normally to the plate. The numerical model is based on the Navier–Stokes and the energy balance equations. The assumed system of equations is solved using the Boussinesq approximation. It is shown that the presence of a three-dimensional obstacle (cylinder) on the plate results in the formation of a complex vortex structure both upstream and downstream of the cylinder. In particular, a horseshoe vortex formed upstream of it is similar to vortex formation that has been observed in forced convection heat transfer by many researchers. In this paper, the tentative results of the study of the complex three-dimensional vortical structure in conditions of free-convection and its influence on the heat transfer are presented.

Key words: numerical modeling; natural convection heat transfer; vortex structure; horseshoe vortex system; heat transfer coefficient

Citation: Yu.S. Chumakov, A.M. Levchenya, H. Malah, The vortex structure formation around a circular cylinder placed on a vertical heated plate, St. Petersburg Polytechnical State University Journal. Physics and Mathematics. 11 (1) (2018) 56 – 66. DOI: 10.18721/JPM.11108

Introduction

The past two decades have seen an increased interest in the flows arising when the boundary layer interacts with different obstacles on the surface along which these flows develop. Flow over an obstacle initiates an adverse pressure gradient causing the separation of the boundary layer. The formation of a rather complex vortex structure and, primarily, the formation of the so-called horseshoe vortex (HSV) is typical for these flows [1].

This type of flows includes forced convection flows arising in the wing/body junction of aircraft, in endwall regions of turbine cascades, in different heat exchange units of complex geometry. The increased pressure region in these flows is stretched along the entire height of the obstacle over which the external flow is incoming, so the separation of the boundary layer and the emerging HSV are very intense. A review of numerous experimental studies that were carried out before the 21st century and dedicated to HSV forms in forced convection flows is presented in [2], and studies of the last fifteen years are briefly reviewed in a recent experimental work [3].

Developing vortex structures obviously have a noticeable effect on exchange processes in the flow, and, if there is a temperature difference between the flow and the streamlined surface, can contribute to significant non-uniformities of local heat transfer. There is a whole class of heat exchange devices where heat exchange occurs under free-convection conditions. For example, one of the models of such heat exchangers can be represented, as a vertical heated plate with a free-convection boundary layer developing along it. Various devices whose temperature is equal to or different from the surface temperature can be mounted on the plate. A strong pressure gradient in the narrow region where the free-convection boundary layer approaches the obstacle leads to separation of the boundary layer. Thus, it can be assumed that, similar to forced convection flow, a complex vortex structure containing a horseshoe-shaped vortex can develop on the plate in the vicinity of the leading edge of the obstacle. The behavior of the flow in this case is determined not only by the intensity of the separation, but also by buoyancy forces acting on the heated flow pushed away from the plate.

The current research in the field of computational fluid dynamics is focused on using numerical simulation techniques for

computing essentially three-dimensional flows with horseshoe vortex structures in forced convection boundary layers (see, for example, Refs. [4, 5]). Successful computation of heat transfer in devices with flow of a free-convection boundary layer over an obstacle largely depends on accurately reproducing the complex dynamic structure of vortex formations both directly in the region where the obstacles approach the surface and in their wake. It should be borne in mind that the flow itself arises from a locally acting body force and is not affected by incoming flow. Unfortunately, we have been unable to uncover any experimental or computational studies on horseshoe vortices in free-convection flow. Ref. [6] is dedicated to analysis of unsteady free convection near a vertical surface under local perturbation due to a small cubic obstacle mounted on the wall. The authors established that the presence of a cylinder immersed in a free-convection boundary layer intensifies heat transfer.

In this paper, we present the results of numerical simulation of a three-dimensional free-convection flow occurring near a vertical heated plate with a circular cylinder placed on it; the axis of the cylinder is directed normally to the surface.

Problem definition

A laminar flow of a viscous incompressible fluid was considered in the Boussinesq approximation in the vicinity of a circular cylinder mounted on a rectangular vertical plane surface (referred to as a plate from now on). The plate was heated relative to the medium that filled the external environment. The air near the plate moved up under the action of a buoyancy force emerging in the gravitational field and formed a free-convection boundary layer along the plate. The surfaces of the plate and the cylinder served as the boundaries of the computational domain; conjugate heat transfer was not simulated. Two parameters of the problem changed in the process of variant (parametric) computations: the temperature of the cylinder and its height.

The goal of the study was to analyze the influence of cylinder heating on the structure of three-dimensional free-convection flow near the junction of the cylinder and the plate, and also to compare the characteristics of the flow and the heat transfer in cases when the cylinder was completely immersed in the boundary layer and when the cylinder height exceeded the thickness of the boundary layer.

Fig. 1 shows a schematic of the computational domain and the coordinate system, as well as the boundary conditions (described below). The origin of the coordinate system is located 0.8 m from the trailing edge of the plate and coincides with the center of the base of the cylinder, the X axis corresponds to the horizontal direction, the Y axis to the vertical one (in the direction of flow), and the Z axis is perpendicular to the plate.

The diameter of the cylinder $D = 0.02$ m. The computational domain was a parallelepiped with the height of $120D$, the width of $25D$ and the thickness of $10D$. All computations were performed with artificial symmetrization of the flow in a plane parallel to the action of gravity, which divides the cylinder in half along its axis. The distance from the cylinder axis to the bottom boundary of the computational domain is $50D$, and $70D$ to the top boundary (see Fig. 1). The height of the cylinder removed (cut off) from the computational domain varies in the simulations (the specific values are given in Table 1).

The boundary conditions are shown in Fig. 1 and were formulated as follows. Surfaces of the plate and the cylinder were solid walls (colored gray) with the no-slip condition imposed. The temperature of the plate was 60°C for all variants computed, and the surface temperature of the cylinder was set according to Table 1. The no-slip condition was also imposed on the bottom and top boundaries of the domain, with the temperature equal to the surrounding medium temperature of 20°C. The symmetry conditions were imposed on the plane separating the cylinder in half along its axis, parallel to its outer boundary. The symmetry condition was also imposed in the $10D$-long sections before and after the plate (in the vertical direction), ensuring impermeability and zero shear in these regions. The boundary parallel to the plate was permeable: the flow could move through it, both inward ejected by the boundary layer (in this case the temperature of the flowing air was 20°C), and outward,

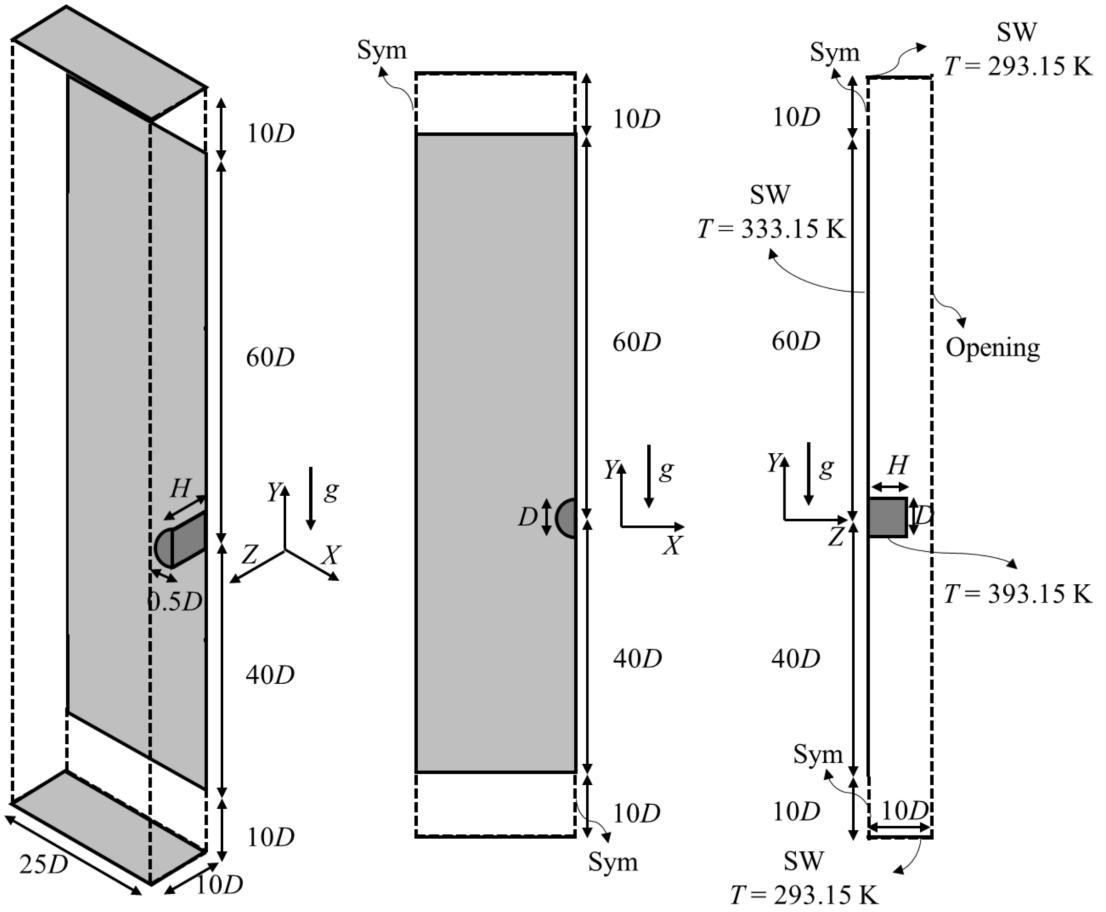

Fig. 1. Geometry of the computational domain in numerical simulation:
H and *D* are the cylinder's height and diameter, respectively *g* is the acceleration of gravity, *T* is the temperature, Sym is the symmetry, SW are the solid walls (colored gray), Opening is the permeable boundary

being pushed out by the streamlined obstacle.

Body-fitted computational grids were used for numerical simulation. The grids were more refined near solid surfaces and in the entire vicinity of the obstacle to improve the resolution quality of horseshoe vortex structures. The grid was clustered to solid walls with a clustering factor of 1.05. Block-structured grids consisting of quadrilaterals with rectangular cells were constructed in the plane of the plate away from the obstacle. A grid block in the vicinity of the cylinder was a *C*-grid in the form of a 'screw-nut' enclosing the cylinder (Fig. 2). Additional grid blocks between the refined grid in the

Table 1

Configurations and heating modes considered

Computational variant	Dimensionless cylinder height (H/D)	Cylinder surface temperature, °C
B-1-60	1	60
B-1-120	1	120
B-5-60	5	60
B-5-120	5	120

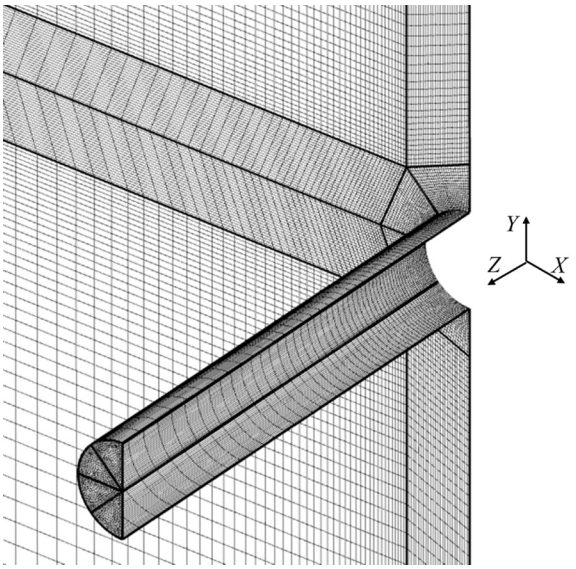

Fig. 2. Fragment of the computational grid near the cylinder

vicinity of the cylinder and a coarser outer region served to smooth the shape and equalize the size of the cells. Such a configuration of the subdomains was chosen to ensure efficient refinement of the grid in the region that interested us without forming strongly skewed or stretched cells, which could occur if a single grid structure was used for the entire computational domain. The resulting grid in the plane of the plate consisted of approximately 50,000 cells. The grid was clustered in the *YZ* plane in the vicinity of the cylinder in such a way that the cell size in the region where the horseshoe vortex developed was 50 times smaller than the diameter *D* of the cylinder. In the direction normal to the plate, the grid consisted of 73 cells with clustering to the plate and to the trailing edge of the cylinder. Three-dimensional grids were obtained by translating the original grid in the direction normal to the plate. The size of a near-wall cell was $0.014D$, and 31 cells fell inside the boundary layer unperturbed by the cylinder. The cell size in the inner block inside the region where the HSV developed was $0.014 - 0.040D$. The cell sizes did not exceed $0.3D$ in any direction throughout the computational domain. The dimension of the resulting three-dimensional grid was about 3.6 million cells.

The commercial package ANSYS FLUENT 16.2 [7] was used for computations in the study. The solution of the Navier – Stokes and the energy equations was obtained using a coupled algorithm. The discretization of the governing equations was carried out with a second order of accuracy for all spatial derivatives.

The difficulties arising in simulation of free-convection flows are primarily due to relatively small velocities of motion and having to simultaneously solve the equations of motion and energy, which makes the numerical model less stable than in simulation of forced convection. The small inertia of the flow and the close relationship between the equations of motion and energy entail performing a larger number of iterations to obtain a converged solution in the computations. The number of iterations in our computations ranged from 1350 to 1600, and the balance accuracy was up to 10^{-6}.

Results and analysis

As a result of the computations, we have obtained steady-state solutions for the four variants listed in Table 1. The results in the vicinity of the cylinder mounted on the plate are of particular interest. The presence of this cylinder completely broke down the incoming flow and turned a two-dimensional free-convection boundary layer into three-dimensional flow, which ultimately had a significant effect on heat transfer.

The structure of the flow in case of forced convection is generally governed by the parameters of the incoming flow, while heat exchange within the model of an incompressible fluid has no effect on the flow field. At the same time, the flow under free convection is generated by the action of the buoyancy force whose intensity depends on the local temperature difference. To assess the effect of the cylinder on the breakdown of the incoming two-dimensional free-convection boundary layer and the resulting development of an extensive region of a three-dimensional vortex flow, it seems expedient to start analyzing the results by determining the boundaries of the temperature inhomogeneity in the vicinity of the cylinder. To this end, a 2 % thickness of the region with temperature non-uniformities was determined for each computational vari-

Table 2

The results of estimating the width of the perturbation region

Computational variant	Width of the perturbation region (X/D)
B-1-60	2.25
B-1-120	2.25
B-5-60	2.50
B-5-120	2.40

ant in different longitudinal cross-sections *YZ* (X = const is chosen), referred to as the near-wall region from now on. This thickness, denoted as δ below, is the coordinate in the *YZ* plane where the local temperature differs from the temperature at the outer boundary of the computational domain by 2 %.

By comparing the results obtained with the corresponding thickness of the unperturbed boundary layer, we determined the extent of the region where the cylinder had an influence on the two-dimensional boundary layer. Table 2, in particular, lists the dimensions of the region of the cylinder's influence at the level of the horizontal line $Y = 0$, along the X axis from the surface of the cylinder.

It follows from Table 2 that an increase in the surface temperature of a short cylinder did not affect the width of the perturbation region of the temperature field (variants B-1-60 and B-1-120) but reduced the size of this region in case of a long cylinder (B-5-60, B -5-120). We should also note that increasing the height of the cylinder resulted in an expansion of the perturbation region, regardless of cylinder heating.

Fig. 3 shows comparisons of the 2% thicknesses of the unperturbed two-dimensional boundary layer with their magnitude in the presence of an obstacle (the cylinder) along the plate on the symmetry line ($X = 0$). Notably, the maximum computed thickness of the temperature boundary layer developing on the vertical heated plate without an obstacle is approximately 0.022 – 0.025 m.

Analysis of the curves in Fig. 3 reveals the following:

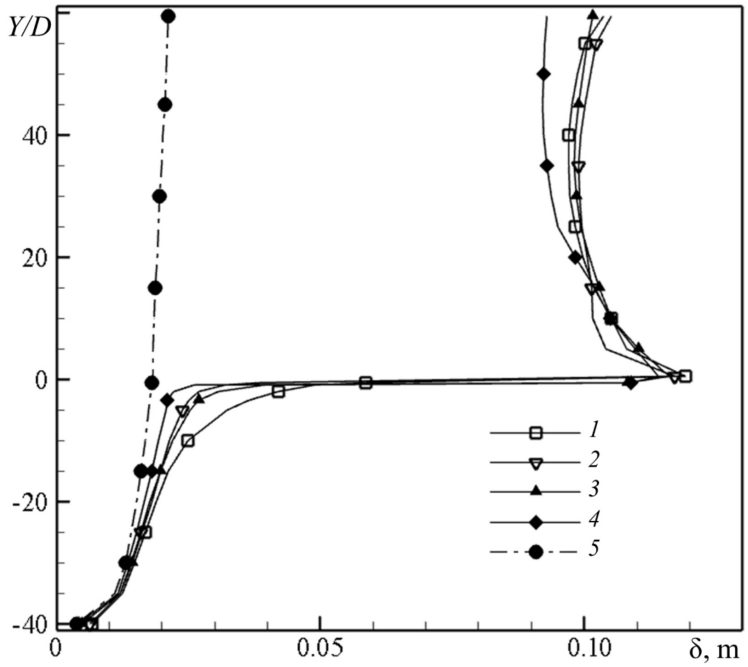

Fig. 3. Distributions of the 2 % thickness of the near-wall region δ as a function of the Y/D coordinate, obtained for different variants: B-1-60 (1), B-1-120 (2), B-5-60 (3), B-5-120 (4) (see Table 1);
the distribution in the absence of the cylinder (5) is also shown

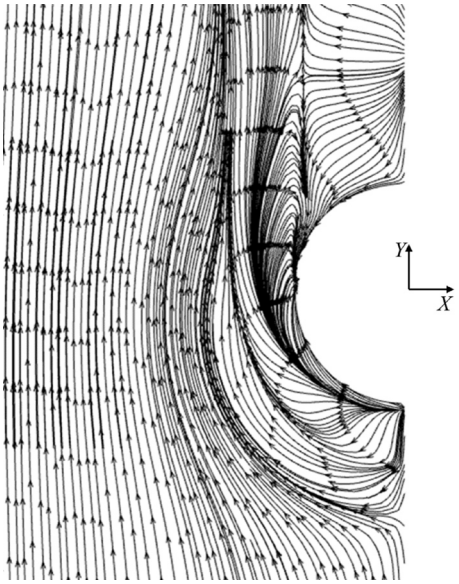

Fig. 4. Surface streaklines on the plate for variant B-1-60 (see Table 1)

the effect of the obstacle spread rather far upstream; the influence of the cylinder on the thickness of the wall layer was already noticeable at a distance $Y/D = -35$, and this influence was greater in case of a short cylinder;

increasing the temperature of the cylinder slightly reduced the degree of influence on the upstream flow;

the thicknesses of the wall layer in the region downstream of the cylinder were practically the same for all variants except variant B-5-120, for which some decrease in thickness was observed. The reason for this behavior was possibly that a long heated cylinder extending beyond the wall layer initiated its own free-convection flow, thus affecting the flow near the surface.

Let us analyze in more detail the flow field in the region of juncture of the cylinder and the plate.

The surface streaklines on the plate near

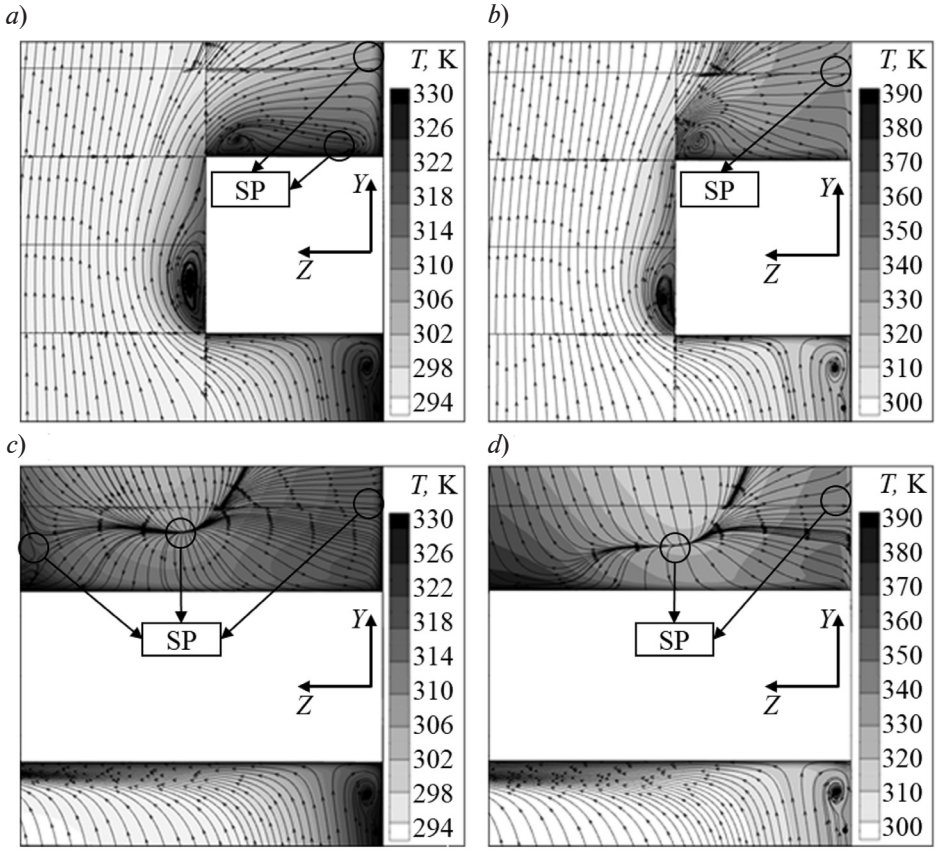

Fig. 5. Volume streamlines and temperature contours (as shades of gray) in the symmetry plane *YZ* for computational variants B-1-60 (*a*), B-1-120 (*b*), B-5-60 (*c*), B-5-120 (*d*) (see Table 1); SP are singular points

the cylinder for variant B-1-60 are shown in Fig. 4. This can be regarded as a picture of the vortex structures developed, allowing to identify the line of separation of the boundary layer upstream of the cylinder, with horseshoe vortices inside the line encircling the obstacle. Traces of the corner vortex developing in front of the cylinder and the development of the entire structure in the wake of the obstacle are visible near the cylinder.

Fragments of streamlines with the temperature fields (as shades of gray) are shown in Fig. 5 in the plane of symmetry *YZ* ($X = 0$). Comparing different modes allows analyzing the effect of the height of the cylinder and its overheating relative to the medium on the dimensions of the HSV. Vortices can be detected in the corner of the junction of the cylinder and the plate in each figure: the primary (more intense) and secondary (weak) HSV; the secondary vortex was located upstream of the primary one, formed as a result of separation of the free-convection boundary layer along the plate. The HSV sizes were similar for all computational variants. A vortex developed in the trailing edge of the cylinder is visible for the cases of flow around a short cylinder (Fig. 5, *a*, *b*). Its axis shifted upstream (towards the cylinder) as its surface temperature increased. A complex vortex structure was formed downstream of the obstacle: for a short cylinder, this was a concentrated vortex (recirculation bubble). The swirling flows inside the vortices stirred and diffused the heated air, changing the heat transfer on the surface of the plate and the cylinder mounted on it.

Several singular points (SP in Fig. 5) were present in the cylinder's wake for all four cases considered, allowing to draw an analogy with a tornado [8]. These singularities drew the fluid particles upstream, along the plate, shifting downstream as the surface temperature of the cylinder and its height increased. Fig. 6 shows tornado-shaped vortices for variant B-5-120. When the height of the cylinder increased and its surface temperature decreased, the base of the vortex funnel moved away from the cylinder's symmetry plane along the *x* axis.

The primary and secondary horseshoe vortices merged together and formed a single

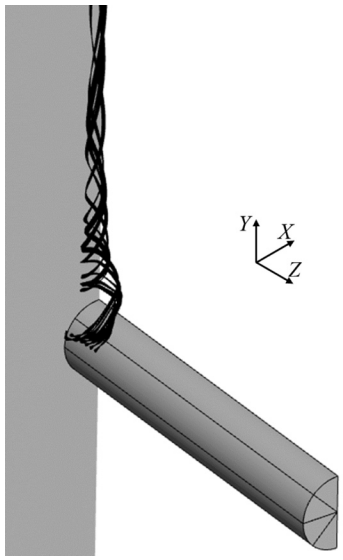

Fig. 6. Streamlines in the trailing edge of the cylinder (variant B-5-120)

structure that slowly moved towards the cylinder, and ultimately contributed to the development of the HSV system [9] (Fig. 7).

A *Q*-criterion [10] was used to visualize three-dimensional vortex structures in Fig. 7; this criterion is defined as follows:

$$Q = \frac{1}{2}(\Omega_{ij}\Omega_{ij} - S_{ij}S_{ij}), \qquad (2)$$

where Ω_{ij} and S_{ij} are the antisymmetric and symmetric parts of the second invariant of the velocity gradient tensor, respectively.

According to [10], vortex structures can be found in regions where $Q > 0$, when the local rotation speed exceeds the strain rate. Comparing the distributions of the *Q*-criterion near the surface of the cylinder and in the region of the junction of the cylinder and the plate for each computational variant (Fig. 7) yields data on the topology and intensity of the vortex structures.

We should note that the HSV systems that developed in the computations with coinciding cylinder heights were identical in shape but had different sizes of the leg of the primary HSV and different intensities, while an increase in the *Q*-criterion was observed over the entire height of the cylinder for the fourth variant. Regardless of the height of the cylinder, as its temperature increased, the isosurface of the

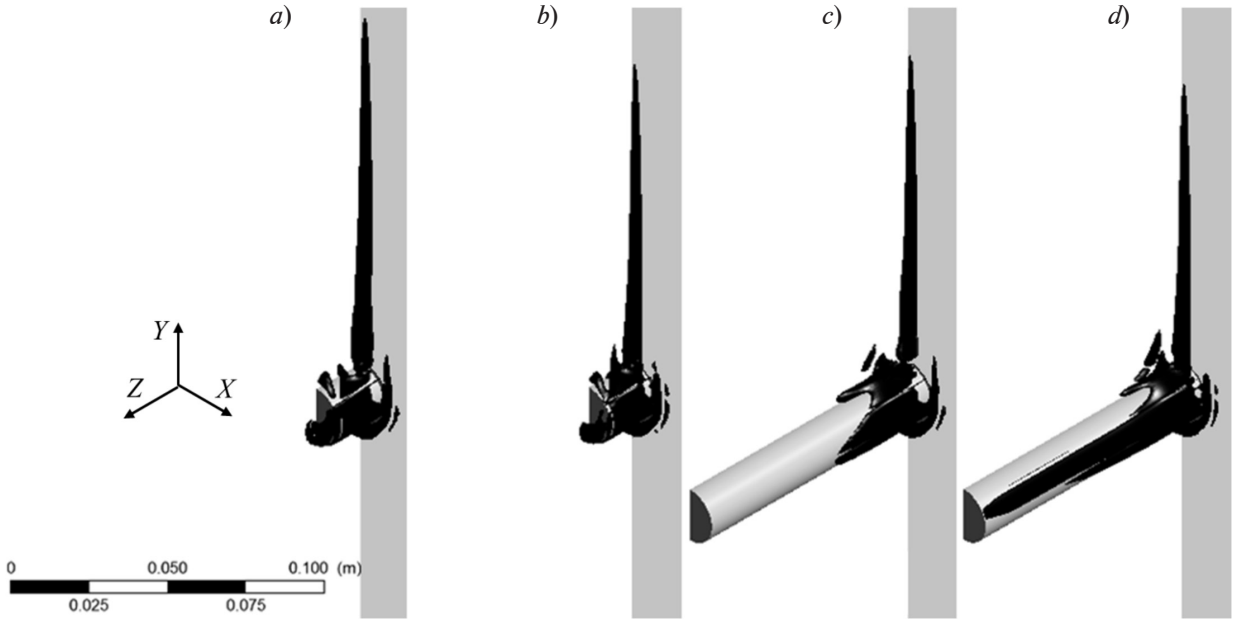

Fig. 7. Visualization of the vortex flow structure around the cylinder using the Q-criterion isosurfaces for variants B-1-60 (*a*), B-1-120 (*b*), B-5-60 (*c*), B-5-120 (*d*)

Q-criterion stretched along the entire height of the cylinder, covering its lateral surface completely, corresponding to intensification of the vortex structures. The legs of the primary HSV in the cylinder's wake reduced in size with an increase in surface temperature of the cylinder and in its height.

A brief analysis of the flow in the vicinity of the junction of the cylinder and the plate and in the wake of the cylinder indicates the formation of a very complex vortex structure contributing to intense mixing of cold and hot air, which undoubtedly had a significant effect on heat exchange in this region. To analyze the effect on heat transfer of three-dimensional vortex flow, it is convenient to use the heat transfer coefficient α, which is defined as follows:

$$\alpha = q / \Delta T,$$

where q is the heat flux from the wall, ΔT is temperature difference between the wall and the external environment.

The distributions of the heat transfer coefficient along the polygonal line made by intersection of the symmetry plane and the solid walls are shown for all computational variants in Fig. 8. The figure consists of three separate spatially related graphs, each of them showing one or two families of curves.

The lower graph shows two families of curves. The first is the distribution of the quantity α (Y/D) along the section of the plate under the cylinder (upstream of it); the vertical axis of the graph serves as the coordinate axis, and the α values are plotted horizontally. These distributions coincide for different computational variants, while the value of α decreases monotonically as the boundary layer develops on the plate, right up to the region directly in front of the cylinder ($Y/D > -1$) where a horseshoe vortex is formed and monotonicity is violated.

It should be noted that the distributions of the heat transfer coefficient obtained in the computations for the region upstream of the cylinder and away from it (i.e., in the region of the unperturbed free-convection boundary layer) are consistent with the data available in the literature. The criterial relation between the local Nusselt number and the local Grashof number has the form of a power function with an exponent close to the value of 1/4, standard for laminar flow near a vertical heated plate [11].

The second family of curves on the lower

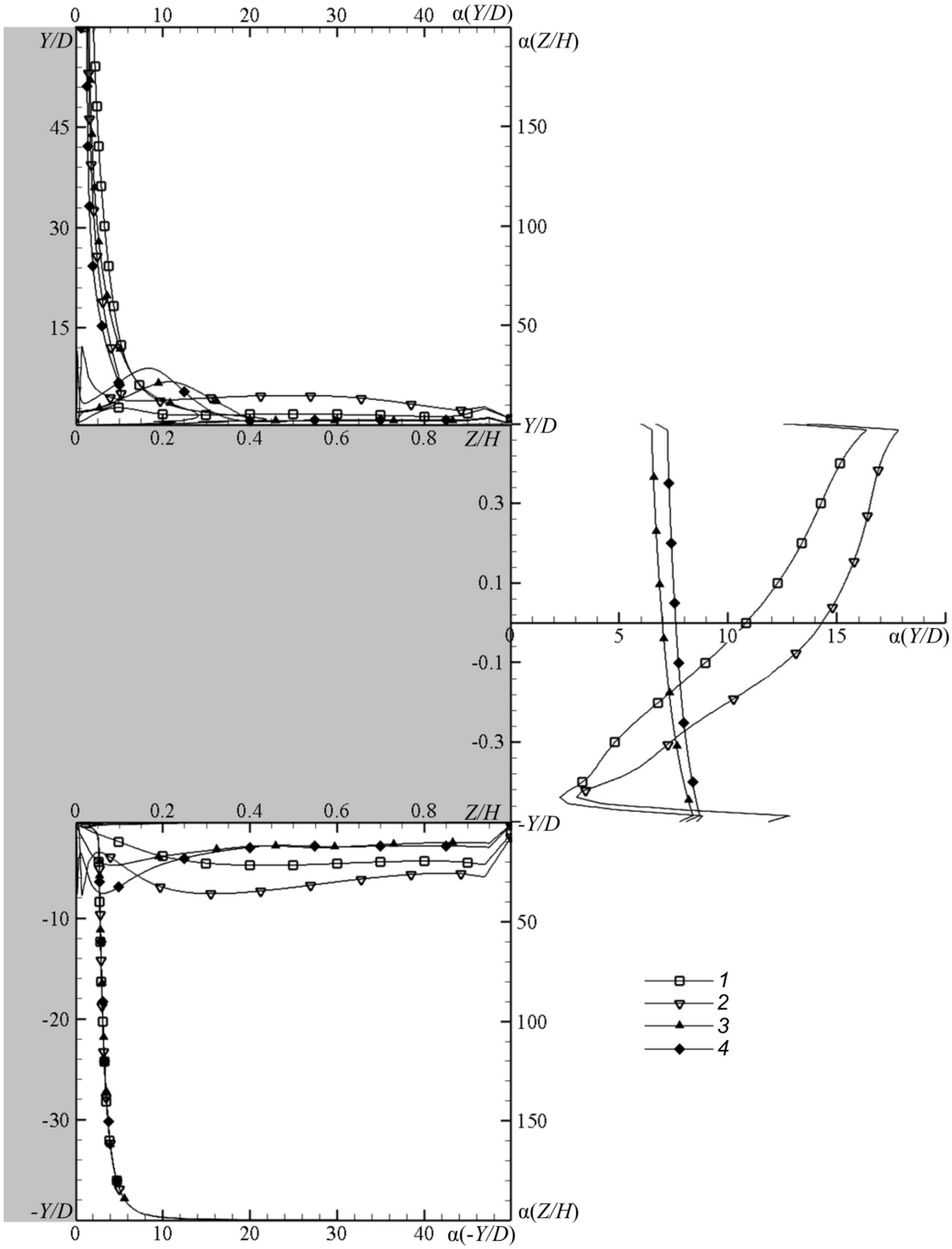

Fig. 8. Distributions of the heat transfer coefficient α along the line of intersection of the symmetry plane (*YZ*) and solid surfaces for computational variants B-1-60 (*a*), B-1-120 (*b*), B-5-60 (*c*), B-5-120 (*d*) (see Table 1)

graph corresponds to the distribution of the heat transfer coefficient along the height of the cylinder, along its leading edge: the coordinate axes change places in accordance with the spatial orientation. The heat transfer coefficient on the lateral surface of the cylinder virtually does not change along the cylinder, while the average level of the coefficient α for a short cylinder slightly increases with increasing surface temperature.

We should note that an increase in the surface temperature leads to a pronounced nonmonotonic change in the coefficient α in the vicinity of the junction of the cylinder and the plate for cylinders of different heights. This circumstance is of course due to intense development of the vortex structure in this region. Similar behavior of the heat transfer coefficient is also characteristic for the distribution of α along the trailing edge of the cylinder (see the upper graph, the dependences $\alpha\,(Y/D)$).

The graph in the middle shows the distributions of the value of α along the diameter of the upper edge of the cylinder. A general tendency to an increase in the heat transfer coefficient can be observed with an increase in the surface temperature of the cylinder. However, while the coefficient α is practically constant for a long cylinder, the heat transfer coefficient increases several times in the downstream direction for a short cylinder completely immersed in the boundary layer. The distributions of the heat transfer coefficient in the region in the cylinder's wake, along the surface of the plate (the upper graph, the dependence $\alpha\,(Z/H)$), are similar for different variants, exhibiting a slow, almost monotonic decrease in heat transfer with increasing distance away from the cylinder. The values of α decrease with an increase in both the surface temperature of the cylinder and in its height.

Conclusion

The results of numerical simulation of the interaction of a free-convection boundary layer with a three-dimensional obstacle (cylinder) allow us to draw the following conclusions:

the assumption that a complex vortex structure with a horseshoe vortex develops in the leading edge of a cylinder located on a vertical plate was confirmed for the case of free-convection flow;

the height of the cylinder has a significant effect on the formation of the vortex zone if it is commensurable with the thickness of the boundary layer;

cylinder overheating compared to the plate temperature has little effect on the upstream flow, but has a marked effect on the flow downstream of the cylinder;

the effect of cylinder overheating is apparently even more pronounced if the height of the cylinder exceeds the thickness of the boundary layer, since in this case the cylinder is an independent source of a free-convection flow, which can significantly affect the downstream flow under certain conditions;

finally, (this, perhaps, is the most important practical conclusion), the heat exchange of the plate (together with the cylinder) with the surrounding air is largely governed by the vortex structure of the flow near the plate, and, consequently, successful computation of the heat exchange largely depends on the accuracy of predicting the dynamic structure of the flow.

REFERENCES

[1] **C.D. Anderson, S.P. Lynch,** Time resolved stereo-PIV measurements of the horseshoe vortex system in a low aspect ratio pin-fin array, AIAA Propulsion and Energy Forum. Orlando, FL, USA (2015) 3733.

[2] **F. Ballio, C. Bettoni, S. Franzetti,** A survey of time-averaged characteristics of laminar and turbulent horseshoe vortices, ASME Journal of Fluids Engineering. 120 (2) (1998) 233–242.

[3] **N. Apsilidis, P. Diplas, C.L. Dancey, P. Bouratsis,** Time-resolved flow dynamics and Reynolds number effects at a wall-cylinder junction, Journal of Fluid Mechanics. 776 (2015) 475–511.

[4] **M.R. Visbal,** Structure of laminar juncture flows, AIAA Journal. 29 (8) (1991) 1273–1282.

[5] **A.M. Levchenya,** Chislennoye modelirovaniye trekhmernogo potoka, obtekayushchego krugovoy tsilindr v oblasti yego sochleneniya s gladkoy stenkoy [Numerical simulation of a 3D flow around a circular cylinder in its overlapping area with a smooth wall], In: Vserossiyskiy seminar po aerogidrodinamike, posvyashchennyy 90-letiyu so dnya rozhdeniya S.V. Vallandera: izbrannyye trudy vserossiyskogo seminara [The All-Russian seminar on aerodynamics on the occasion of 90th anniversary of S.V. Vallander: Selecta from The All-Russian seminar] , St. Petersburg, SPbSU (2008) 64–69.

[6] **G. Polidori, J. Padet,** Flow visualization and free convection heat transfer at the junction of short cylinders mounted on a heated wall, Journal of Flow Visualization and Image Processing. 10 (2003) 13–26.

[7] ANSYS Academic Research Mechanical, Release 16.2, Help System, Fluent Theory Guide,

ANSYS, Inc. 2015.

[8] **G. Kirkil, G. Constantinescu,** Effects of cylinder Reynolds number on the turbulent horseshoe vortex system and near wake of a surface-mounted circular cylinder, Physics of Fluids. 27 (7) (2015) 075102.

[9] **J.V.S. Tala, S. Russeil, D. Bougeard, J.L. Harion,** Investigation of the flow characteristics in a multirow finned-tube heat exchanger model by means of PIV measurements, Experimental Thermal and Fluid Science. 50 (2013) 45–53.

[10] **J.C.R. Hunt, A.A. Wray, P. Moin,** Eddies, stream, and convergence zones in turbulent flows, Center for Turbulence Research Report (CTR-S88). (1988) 193–208.

[11] **V.A. Kuzmitskii, Yu.S. Chumakov,** Analysis of characteristics of flow under conditions of laminar-to-turdulent transition in a free-convection boundary layer, High Temperature. 37(2) (1999) 247–253.

Received 06.11.2017, accepted 05.12.2017.

THE AUTHORS

CHUMAKOV Yurii S.
Peter the Great St. Petersburg Polytechnic University
29 Politechnicheskaya St., St. Petersburg, 195251, Russian Federation
chymakov@yahoo.com

LEVCHENYA Alexander M.
Peter the Great St. Petersburg Polytechnic University
29 Politechnicheskaya St., St. Petersburg, 195251, Russian Federation
levchenya_am@spbstu.ru

MALAH Hamid
Peter the Great St. Petersburg Polytechnic University
29 Politechnicheskaya St., St. Petersburg, 195251, Russian Federation
hamid.malah@gmail.com